Materials Science & Engineering A 880 (2023) 145272

Contents lists available at ScienceDirect

Materials Science & Engineering A

journal homepage: www.elsevier.com/locate/msea

Effect of inter layer cold work on 2024 aluminium alloy produced by wire directed energy deposition

E. Eimer [a,*], S. Ganguly [a], S. Czink [b], S. Dietrich [b], B. Chehab [c], J. Ding [a], S. Williams [a]

[a] Cranfield Univeristy, College Road, MK430AL, United Kingdom
[b] Karlsruher Institut für Technologie, Kaiserstraße 12, 76131, Karlsruhe, Germany
[c] Constellium Technology Center, 725 Rue Aristide Berges, 38341, Voreppe, France

ARTICLE INFO

Keywords:
Wire-DED
Additive manufacturing
Aluminium copper
Cold work
Heat treatment

ABSTRACT

Aluminium copper magnesium alloys are widely used in the aerospace sector. Wire-based Directed Energy Deposition could replace conventional manufacturing routes to build large and semi-complex components for this industry if high mechanical performance can be achieved in the deposit.

The scope of this study was to assess the effect of inter-pass rolling on a 2024 aluminium alloy wire-based DED built structure and to investigate the impact of cold work during the deposition process on the microstructure and mechanical performances. The 2024 aluminium alloy was deposited using two variants of gas metal arc process, and the effects of the deposition process, cold work and heat treatment were studied using macro and micro-structural observations, hardness measurement and tensile tests. The material response to inter-pass rolling and the formation of rolling defects was found to depend on the deposition process variant and bead geometry. While a significant strengthening of the deposit was observed with one process, only a drastic reduction of defects was observed with the second. It was also found that the application of cold work and heat treatment led to lowering of anisotropy and higher ductility when compared with heat-treated deposit without any inter-pass rolling.

1. Introduction

Wire-based Directed Energy Deposition (w-DED), also called Wire and Arc Additive Manufacturing (WAAM) is a process that uses an electric arc as a heat source and wire as feedstock to deposit, layer by layer, metallic components. Contrary to some powder-based processes, WAAM does not have a stringent requirement for gas shielding of the entire deposited structure when unreactive material, such as most aluminium alloys, are processed. Also, a deposition rate of a few kilograms per hour can be achieved: this means that large scale parts can be manufactured by this process in a reasonable time and for a sensible cost [1].

The compatibility between WAAM and aluminium alloys has been investigated for various ranges of chemical compositions. Numerous studies using low to medium strength alloys were reported: aluminium silicon [2] and aluminium magnesium [2–4] alloys are suitable for WAAM because of their favourable solidification behaviour which does not lead to solidification cracking. However, to achieve high strength in w-DED components, high strength precipitation hardened aluminium alloys, such as aluminium copper and aluminium zinc, are required. Aluminium 2024 is an aluminium copper magnesium alloy widely used as a structural alloy in the aerospace sector, especially in aircraft fuselage and wing primary structures, due to its specific strength and damage tolerance properties [5,6]. This alloy is generally considered as un-weldable by fusion processes because of its unfavourable solidification behaviour [7]. However, the possibility to weld this alloy has been demonstrated by Picking et al., by optimising the filler material composition by mixing up to three wires in situ to create a favourable solidification path [8,9]. A similar approach has been used to deposit a wide range of aluminium copper magnesium alloys using WAAM by Qi et al. [10] and Gu et al. [11]. In further publications, the authors demonstrated the possibility of depositing AA2024 using one or two wires, and the properties of 2024 WAAM deposit were also investigated [12,13].

2024 is an age-hardening alloy; its optimum mechanical properties are achieved by heat treatment. During the conventional manufacture of wrought 2024 products, solution treatment, stretching, and ageing are systematically conducted to achieve the maximum strength [14]. Qi et al. showed the effect of solution treatment on the properties of WAAM 2024 [13,15]. Inter-pass rolling is another processing route used to

* Corresponding author.
E-mail address: e.eimer@cranfield.ac.uk (E. Eimer).

https://doi.org/10.1016/j.msea.2023.145272
Received 16 April 2023; Received in revised form 6 June 2023; Accepted 7 June 2023
Available online 19 June 2023

increase the strength of WAAM alloys, as reported by Gu et al. [3,16]. Inter-pass rolling consists of applying load at room temperature on the deposited material in between each deposition pass to introduce localised plastic strain in the deposited material. It enables a significant reduction of the porosity level [17], an increase in mechanical properties [3,16], and a reduction of residual stresses and distortion [18] during the processing of aluminium alloys. Most studies were reported on the use of different rolling parameters on single pass walls [19,20] or more complex geometry [21]. The detailed effects of inter layer rolling on aluminium deposit identified in the literature are the following:

1. Gu et al. [16] attributed the increase of tensile properties of AA2319 WAAM deposit during inter-pass rolling to high-density dislocations and fine sub-grains with relatively low misorientations. A high concentration of θ′ phases was observed using transmission electron microscopy in the heat-treated material, but dislocations were observed only in the rolled material. The rolled material hardness was 102 HV, which was higher than the as-deposited material hardness, 68 HV, but lower than the hardness value of 144 HV obtained after heat treatment. The elongation at rupture of the rolled samples, in vertical orientation was slightly lower than for the horizontal orientation (7.3% vs 8.5%).
2. Honnige et al. [18] showed that the lattice parameter of WAAM 2319 increases with the rolling load. The authors suggested that the correlation between lattice parameter and rolling could be caused by a reduction of solutionised copper content in the matrix of the rolled material due to extensive precipitation. Dislocations are indeed well-known nucleation sites for Guinier Preston zones and thereby for precipitates. Many precipitation hardening aluminium alloy products exploit this phenomenon and use cold work after solution treatment to promote precipitation and increase the mechanical performances.
3. Gu et al. [3] studied the effect of inter-layer rolling on 5083 WAAM material. The increase in tensile properties was attributed to deformation-induced high-density dislocations and sub-structures and grain refinement. The author did not observe any significant reduction in elongation. This was attributed to the reduction in porosity level, the grain refinement and sub grain formation that contribute to strength increase without significant ductility losses and the repeated recrystallisation promoted during the reheating caused by the layer deposition.
4. Gu et al. [17] investigated the effect of inter-layer rolling on the gas pores and dendritic shrinkage cavities of 2319 and 5083 WAAM material. The authors observed that pores were gradually flattened to oblate spheroids by increasing rolling load. When sufficient rolling load was used, the pores could not be detected by optical microscopy. The authors used the relatively abundant literature on the effect of compressive strain on porosity in aluminium alloy to explain how these defects could be annihilated. They proposed that the hydrogen is trapped in the dislocation produced during the cold work and escapes through dislocation pipes connected to the metal surface, as proposed by Toda et al. [22]. The healing behaviour of microscopic pores is not approved unanimously in the literature but has been observed by several authors. Investigations showed that compressive strain could close certain pores that did not reappear after high-temperature heat treatment. However, certain pores reappeared at their original positions during heat treatment [22]. In wrought products, the flattened porosities during cold work operation is cited as a cause for the reduction in mechanical properties in the out-of-plane direction [23]. However, combining forging and heat treatment was proven beneficial to dissolve hydrogen compressed in the flattened pores [24].

Fixter et al. [12] reported preliminary results on inter-pass rolled WAAM AA2024, but their short study focused on the feasibility of depositing AA2024 using w-DED and only reported tensile properties in the horizontal direction. In this paper, the effect of inter-pass rolling on WAAM AA2024 is extensively investigated: both horizontal and vertical tensile properties are measured. Also, no previous study attempted to correlate the effect of deposition power source characteristics and process parameters on deposit properties after inter-layer rolling: this paper aims to investigate the overall and interdependent effect of deposition process and cold working on the deposit microstructure and mechanical properties.

Two variants of Gas Metal Arc process, viz. the Cold Metal Transfer - Pulse (CMT-P) and Cold Metal Transfer - Pulse Advanced (CMT-P-Adv), developed by Fronius, were used to examine their effects on the as-deposited and as-rolled properties of the 2024 alloy. These processes were chosen because of their common use in aluminium WAAM [16,17,25–27]. The CMT-P process has a higher heat input than CMT-P-Adv, resulting in a wider bead shape and higher penetration. The CMT-P-Adv is an alternative current process designed to clean the oxide layer on the wire surface, resulting in a lower porosity in WAAM deposit [28]. Solutionising and age hardening heat treatment were also conducted to study and correlate the effect of inter-pass rolling for different deposition processes on the age-hardening response of the deposit.

2. Material and methods

Four single bead AA2024 walls were deposited using Cold Metal Transfer -Pulse (CMT-P) and Cold Metal Transfer - Pulse Advanced (CMT-P-Adv) on AA2024 substrates, as indicated in Fig. 1. The walls were 400 mm long, 100 mm high, and their thickness depended on the deposition process and cold work conditions and varied from 6 to 13.3 mm. The chemical composition of the substrate and wire are shown in Table 1. The chemical composition of the wire was determined by Inductively coupled plasma-optical emission spectroscopy (ICP-OES) and the composition of the substrate was taken from the Aluminium Association registry [29]. Inter-pass rolling was applied on two of these walls. It consisted of applying a vertical compressive load, of 45 kN, on each layer, before deposition of the next layer, by a roller of 100 mm diameter. The load was applied by a hydraulic cylinder, as described by Gu et al. [16].

A wire feed speed of 6 m/min and a travel speed of 10 mm/s were used with a contact tip to the work-piece distance of 11 mm. The current and voltage of the arc were measured using a AMV5000 monitor. The values were then used to calculate the instantaneous heat input using an efficiency coefficient of 84% [30]. The calculated point to point average heat input of CMT-P-Adv and CMT-P was 120 and 234 J/mm, respectively. The power source provided the local shielding through the torch, and a flow of 25 L/min of pure argon was used. The dwell time between two successive layer depositions was set at 2 min. Fig. 1 shows a diagram of the eight conditions studied.

Half of each wall was heat treated. As shown in Fig. 2, both horizontal and vertical directions were tested using four specimens.

For the microstructural study, samples from vertical cross-sections, normal to the deposition direction, were cold mounted. The samples were ground using SiC papers under flowing water, and diamond pastes,

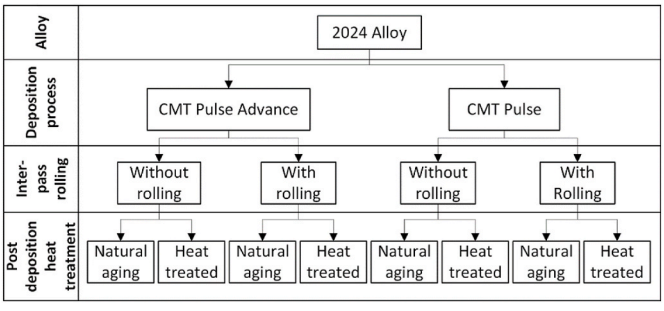

Fig. 1. Diagram of the different conditions tested.

Table 1
Material chemical composition.

	Cu	Mg	Mn	Fe	Si	Zn	Ti	Cr
Wire	4.3	1.39	0.61	0.09	0.03	0.21	0.11	<0.01
Substrate	3.8–4.9	1.2–1.8	0.30–0.9	0.50 Max	0.50 Max	0.25 Max	0.15 Max	0.10 Max

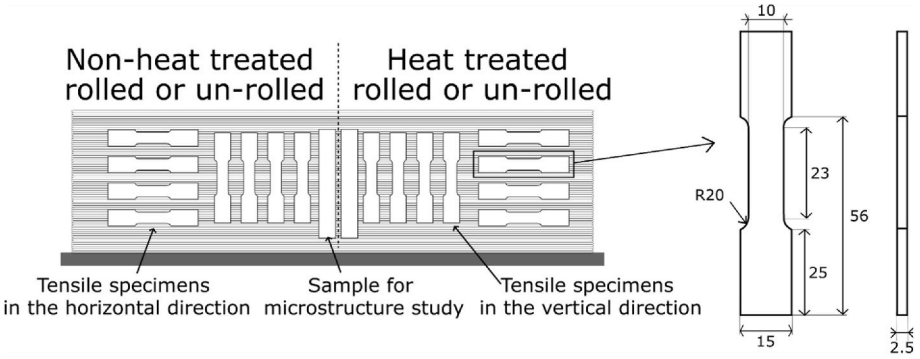

Fig. 2. Samples position in each wall and tensile specimen dimensions.

alumina alpha 0.3 μm and colloidal silica 0.05 μm suspension were used for polishing. Keller's reagent was used as the etchant for optical imaging with a Nikon Optiphot Microscope. Walls cross section and ruptured tensile specimens were observed using a XL30 Environmental Scanning Electron Microscope in backscatter mode, with a working distance of 10.5 mm, a spot size of 6 mm diameter and a voltage of 20 keV. A Zwick Roell Auto-C.A.M.S. machine was used for micro hardness testing, with an indent load of 100 g and time of 15 s.

The porosity of each wall was evaluated in the rolled and un-rolled conditions by micro-computed tomography (μCT). A 5 mm thick and about 20 mm long cross-section was scanned with the μCT-system PRECISION developed by YXLON International GmbH. The X-Ray beam for scanning the samples was generated with an accelerating voltage of 165 kV and a target current of 0.10 mA. A flat panel detector PerkinElmer XRD1620 AN with a pixel pitch of 200 μm and a total size of 2048 × 2048 pixels was used to capture X-ray intensity. Samples were scanned with a focus object distance of 78.5 mm and a focus detector distance of 899.9 mm, resulting in a resolution of 17.5 μm voxel size. The 3D images were reconstructed from the projections with a filtered back projection (FBP) algorithm using VGStudioMAX3.4 by Volume Graphics international GmbH. Projections of the lowest grey values were generated with a thick slab algorithm along 5 mm for a qualitative investigation of the defect distribution. The reconstructed 3D images were segmented by using a local contrast threshold-algorithm with a local domain radius of 10 voxels for the quantitative porosity analysis. Pores with a volume smaller than 2 × 2 × 2 voxels were not considered in the analysis to reduce noise. During the post-treatment, pores were classified according to their volume in segments with an increment of 10^{-4} mm^3.

The wall geometry was characterised for the Total Wall Width (TWW), Effective Wall Width (EWW), Surface Waviness (SW), Layer Height (LH), and remelted depth, as shown in Fig. 3. The remelting depth was determined by subtracting the average layer height from the top layer height. The percentage of deformation after rolling, remelting coefficient, and bead aspect ratio were calculated using the following equation:

$$\%_{deformation} = \left(1 - \frac{Layer\ height_{As-rolled}}{Layer\ height_{As-deposited}}\right) \times 100$$

$$Remelting\ coefficient = \frac{remelted\ depth}{remelted\ depth + Layer\ Height}$$

$$Bead\ aspect\ ratio = \frac{Total\ Wall\ Width}{Layer\ Height}$$

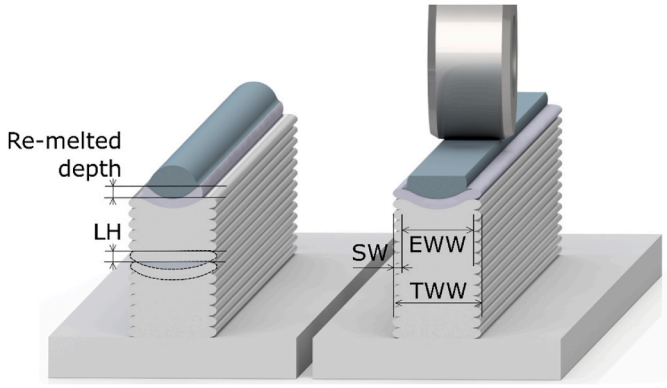

Fig. 3. Schematic of the effect of inter-pass rolling on the wall geometry.

The section of the walls destined to be heat treated were roughly machined to a thickness of 5 mm before heat treatment for the tensile test campaign. A two-step heat treatment, solution treatment and aging, was applied. The solution-treatment at 498 °C for 90 min was chosen to match one of the conditions used by Qi et al. [15] in their study of the effect of solution treatment temperature on 2024 WAAM deposit properties. The latter paper suggested that a solution treatment of 503 °C produce better results, but this option was not selected here, as this temperature is higher than the alloy melting point of 502 °C [31]. The solution treated samples were water quenched and a 10-h aging was carried out at 177 °C. Tensile tests were carried out using an electro-mechanical machine with a 1 mm/min displacement rate; the tensile specimen geometry is given in Fig. 2.

3. Results

3.1. Geometry and macrostructure

Table 2 provides the geometric characteristics and Fig. 3 shows a schematic of the top of the wall after deposition and rolling to illustrate this data. In as-deposited condition, the layer width and re-melting depth are smaller, and the layer height is higher if CMT-P-Adv was used when compared with CMT-P. This lead to a lower bead aspect ratio for the CMT-P-Adv deposit compared to the CMT-P. The surface waviness of the CMT-P wall is lower than that of CMT-P-Adv, showing the

Table 2
Wall geometry.

	TWW [mm]	EWW [mm]	SW [mm]	LH [mm]	Aspect ratio	Re-melting depth [mm]	Re-melting coefficient	%Deformation
CMT-P-Adv								
Un-rolled	6.0	4.2	0.9	2.53	2.4	2	44.1	
Rolled	10.6	8.5	1.1	1.35	7.9	1.3	49	47%
CMT-P								
Un-rolled	10.3	8.9	0.7	1.29	8.0	3.7	74.1	
Rolled	13.3	12.2	0.5	0.93	14.3	1.8	65	28%

former deposition process generated a more regular wall geometry. Inter-pass rolling considerably reduces the layer height and increases the wall width. The percentage of deformation is higher for the material deposited with the CMT-P-Adv than the CMT-P process. This can be explained by the higher aspect ratio of the CMT-P unrolled material, resulting in a larger surface contact between the roller and the top layer leading to lower rolling pressure. The re-melting depth is lower than the LH when CMT-P-Adv process is used but considerably larger than the LH when the CMT-P process is used. Consequently, the remelting coefficient is significantly higher for the CMT-P deposit compared to the CMT-P-Adv deposit.

Fig. 4 (b) shows an example of a defect between two layers, starting near the edge of the CMT-P-Adv rolled wall. These features are scale defects rolled in the material: the thin oxide layer that coated the layer surface get entrapped in between the folds generated by rolling. The formation of this scale has been observed on w-DED INCONEL deposit by Xu et al. [32]. No defects of this nature were observed in the CMT-P rolled wall, as shown in Fig. 4 (a). This can be explained by the difference in bead aspect ratio: when rolling is applied to the high aspect ratio bead deposited by CMT-P, there is no material folding over itself at the wall edges, and the aspect ratio is only marginally impacted by rolling, as shown in Table 2. However, when rolling the CMT-P-Adv wall, the aspect ratio, small to start with, increased significantly. Therefore, folding defects were observed in the CMT-P-Adv wall, and not on the CMT-P wall.

When CMT-P-Adv is used, the SW increases with rolling because it generated bulges near the edges of the layer, as shown in Fig. 4 (b). However, when CMT-P is used, the SW is reduced by rolling. Regardless of the deposition process, inter-pass rolling increases both TWW and EWW.

3.2. Porosity

Fig. 5 provides images of the porosity observed by μCT in a 5 mm thick and wall-width wide volume. These images show all porosity detected in the 5 mm thick material. The total porosity values are given in Table 3. The porosity level in the CMT-P deposit is slightly higher than in the CMT-P-Adv deposit. This is coherent with the literature [28] and can be explained by a combination of the lack of oxide cleaning and a higher heat input during CMT-P deposition. In the non-rolled CMT-P-Adv deposit, pores are distributed homogeneously (Fig. 5 (a)). In contrast, horizontal regions of high porosity concentration, likely caused by the higher remelting depth, are observed in the inter-layer boundary region in the un-rolled CMT-P deposit (Fig. 5 (b)). Inter-layer rolling reduced the porosity level drastically for both deposition processes. In both as-rolled materials, pores mainly are found near the wall edges. This is likely to be caused by uneven pressure distribution and strain field during rolling.

Fig. 6 shows the number of pores found per 100 mm^3 of deposit as a function of the pore volumes. For both deposition processes, the number of detected pores drastically decreases for higher pore volumes and large pores are only detected in the un-rolled material. Inter-pass rolling drastically reduces the number of pores of all size. The effect of heat treatment on porosity level and distribution has been extensively investigated in the literature [17,22,33]. The porosity level is expected to rise in the material that has not been rolled, but no or limited increase in the rolled deposit should be observed. This was not investigated further in this work.

3.2.1. Micro hardness

Table 4 provides the micro hardness results. There is no significant effect of the deposition process on the micro hardness in as-deposited condition. Rolling significantly increases the hardness of the material deposited with the CMT-P-Adv process. This phenomena has been investigated by Gu et al. [16] on 2319 WAAM deposit. The authors characterised the effect of rolling on dislocation density, grain refinement and precipitates size and distribution. They concluded that the most contributing strengthening mechanism of rolling was work hardening, evident from dislocation density increase and sub-grain misorientation. However, rolling do not have any significant effect on the hardness of the samples built with CMT-P process, apart from a slight reduction of the hardness deviation. This absence of strengthening is caused by the numerous remelting cycles annealing the strengthening effect of rolling.

Heat treatment increases the hardness when applied to un-rolled or rolled material. For the CMT-P deposit, the hardness of the heat-treated material is 10HV higher if rolling is carried out. This can be explained by a reduction of defect level, confirmed by the reduction in measurement variation, and by a better response toward heat treatment caused by a lower alloying element segregation after rolling.

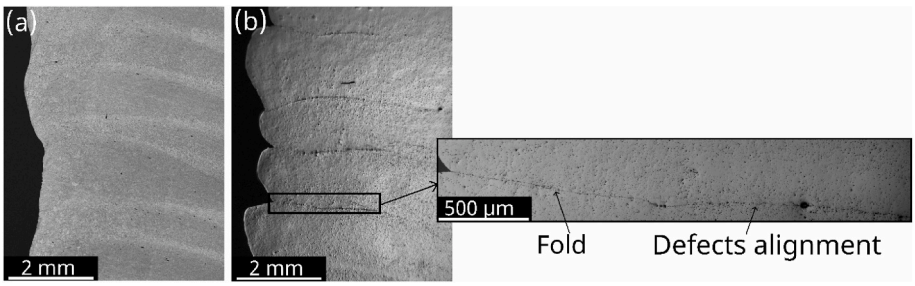

Fig. 4. Layer fold at the edge of the (a) CMT-P and (b) CMT-P-ADV rolled material into the wall.

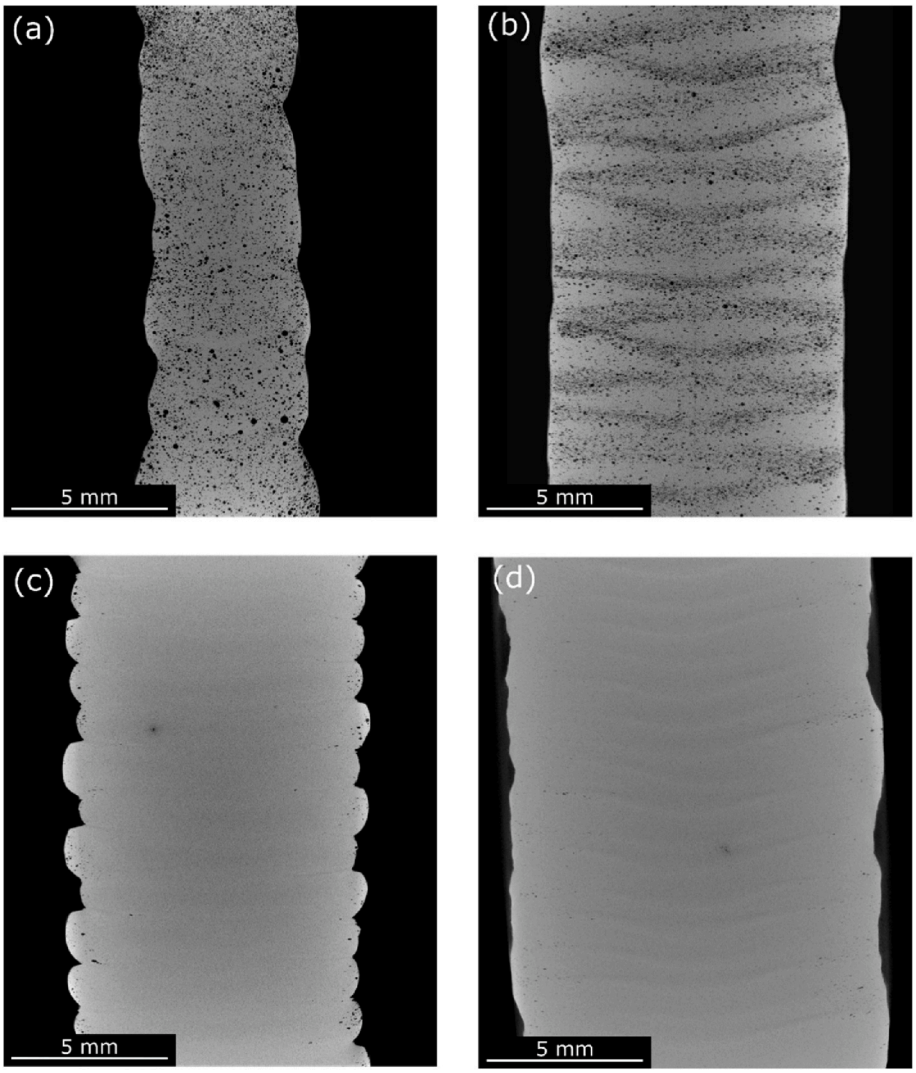

Fig. 5. Porosity detected by 3D tomography in a 5 mm thick cross section of (a) as-deposited CMT-P-Adv, (b) as-deposited CMT-P, (c) as-rolled CMT-P-Adv, and (d) as-rolled CMT-P material.

Table 3
Global porosity results.

	CMP-PAdv	CMT-P
Porosity [%]		
Un-rolled	0,317	0362
Rolled	0,002	0004

3.3. Microstructure

3.3.1. CMT-P-Adv

Fig. 7 shows the microstructures of the material deposited with CMT-P-Adv process. The microstructures in the as-deposited state mainly consists of dendritic equiaxed grains. The SEM image shows that the as-deposited material contains large and coarse copper-rich particles. The chemical composition and nature of these phases were extensively studied by Qi et al. [13]: the low solidification rate of WAAM causes extensive alloying element segregation in the as-deposited condition, resulting in the formation of Al_2Cu and Al_2CuMg with copper and magnesium content up to 22% and 1.6%, respectively.

No significant change in average grain size is observed after heat treatment. The SEM image shows that, after heat treatment, a large quantity of this copper-rich network is solutionised in the matrix.

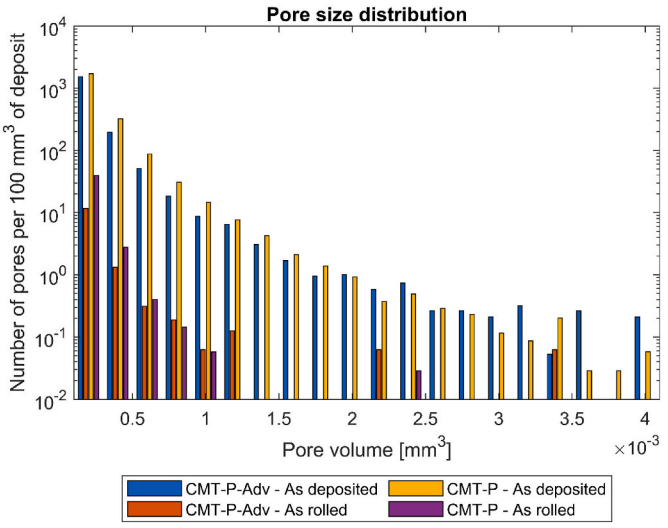

Fig. 6. Pore volume distribution.

The microstructure of the rolled CMT-P-Adv specimen is inhomogeneous: a clear line of coarse equiaxed grains are observed between

Table 4
Vickers Micro hardness results [HV0.1].

		Before heat treatment	After heat treatment
CMT-P-Adv			
	Un-rolled	103 ± 7	140 ± 5
	Rolled	128 ± 5	141 ± 6
CMT-P			
	Un-rolled	100 ± 11	132 ± 12
	Rolled	105 ± 3	142 ± 6

layers, and across the whole wall width in Fig. 7 (g). This can be explained by the low remelting coefficient indicating that only part of a layer is remelted during the deposition of the next one. The rest of the microstructure is composed of equiaxed grains, much smaller than in the un-rolled sample. The SEM image in Fig. 7 (i) shows that the copper-rich particles were fractured and elongated by the rolling load. After heat treatment, the microstructure is more homogeneous, mainly because of partial recrystallisation. It is still possible to observe coarse grain alignment between layers and on the side of the wall. Most of the eutectic compound is solutionised, and the copper-rich particles left are smaller, and lower in volume fraction, than the ones observed in the un-rolled heat-treated sample.

3.3.2. CMT-P

Fig. 8 shows the optical and SEM images of the CMT-P material. The un-rolled microstructure is mainly made of dendritic grains, with some small columnar grains and pore alignments between layers, coherent with the porosity image shown in Fig. 5 (b). The eutectic network is a noticeable difference between the CMT-P and CMT-P-Adv material. In the CMT-P deposit, lack of material in the inter-dendritic region is

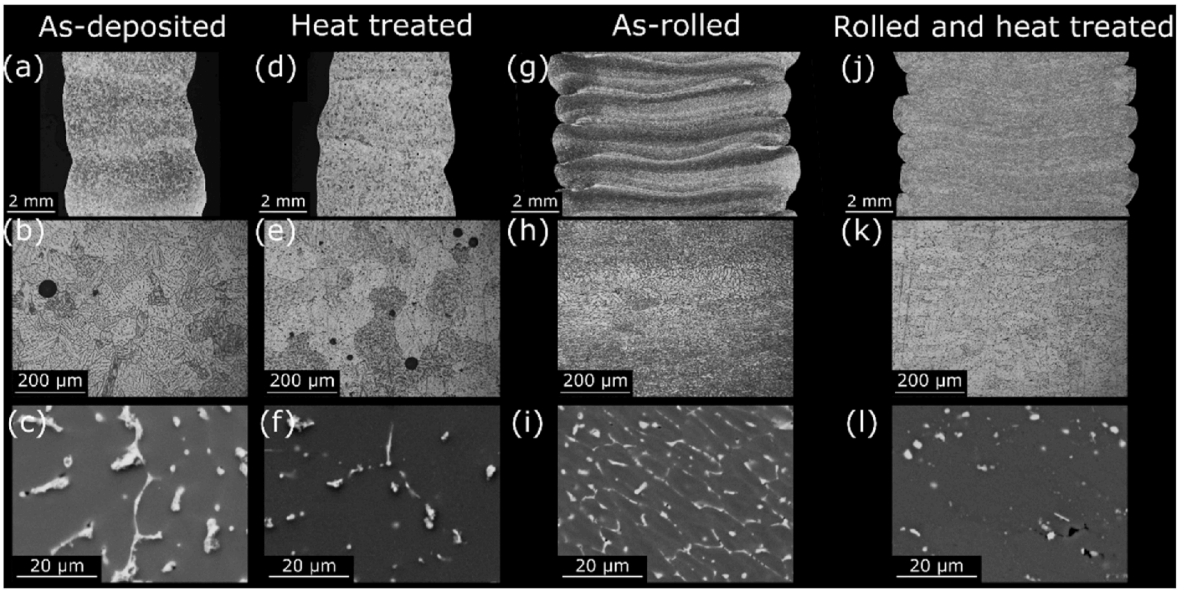

Fig. 7. Optical images of the material deposited with CMT-P-Adv process in the (a, b, & c) as-deposited, (d, e, & f) heat treated, (g, h, & i) as rolled and (j, k, & l) rolled and heat-treated conditions.

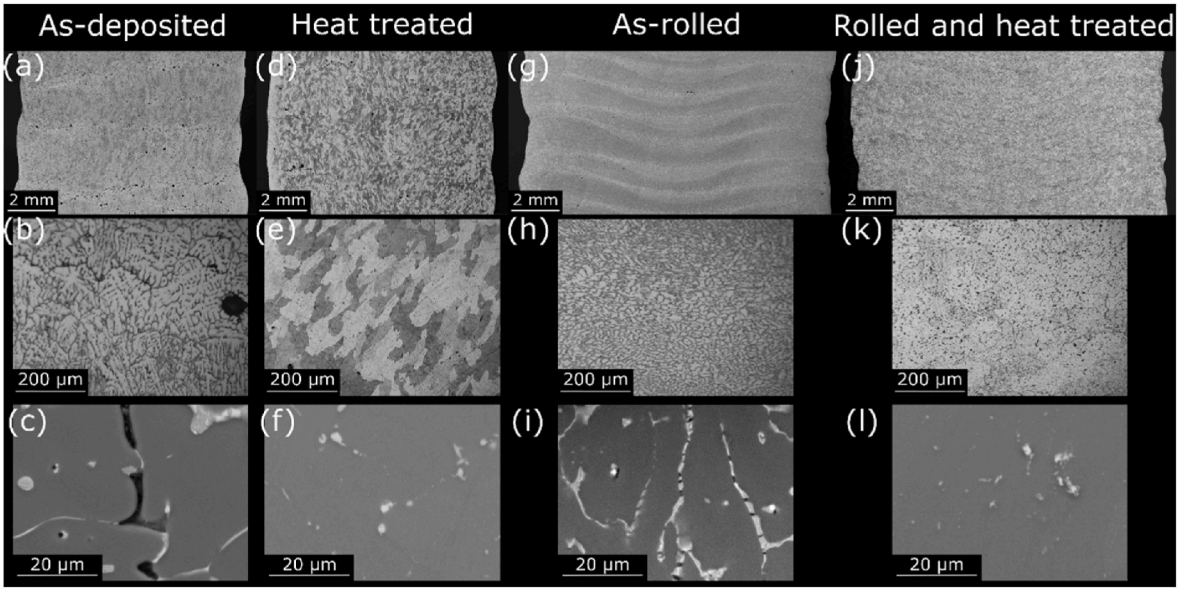

Fig. 8. Optical images of the material deposited with CMT-P process in the (a, b, & c) as-deposited, (d, e, & f) heat treated, (g, h, & i) as-rolled and (j, k, & l) rolled & heat-treated conditions.

visible in Fig. 8 (c). These inter-dendritic voids, or shrinkage porosity, were previously described as a consequence of the difference in solubility of hydrogen between the solid and liquid metal by Talbot [23]. The inter-dendritic porosity in the CMT-P deposit is likely to be caused by the high remelting coefficient, causing the layers to be fully and partially remelted several times. As the material is melted, the eutectic phase captures an additional amount of hydrogen stored in the matrix that generate gas pores during solidification. After heat treatment, large areas are covered by small columnar grains, and the copper-rich network is largely solutionised.

Inter-pass rolling refines the microstructure: tiny equiaxed grain are observed in the middle of the sample. The grains are larger on the edge of the sample. As shown in Fig. 8 (i), the amount of shrinkage porosity observed is drastically reduced. As shown by the SEM image (i), inter-pass rolling reduces the porosity density significantly. It also slightly reduces the size of the secondary phases, but not as significantly as for the CMT-P-Adv rolled sample, as shown in Fig. 7 (i). This is due to a combination of two phenomena: the numerous remelting and reheating cycle, as the size of eutectic phases is heavily impacted by thermal cycle; and the lower deformation rate of the CMT-P material during rolling as reported in Table 2. Nevertheless, rolling elongates and severs the copper-rich phases along the grain boundaries as shown in Fig. 8 (i).

Heat treatment, when carried out on the rolled material, results in grain growth and a relatively uniform microstructure, as shown in Fig. 8 picture (j). The SEM images show that the copper-rich phase distribution is similar when heat treatment is carried out on the un-rolled and rolled material.

3.4. Tensile test results

Figs. 9 and 10 provide the average Proof Stress (PS), Ultimate Tensile Strength (UTS) and elongation at break for each tested condition. The data used in these two plots are given in Table 5.

In as-deposited condition, a strong anisotropy is observed, regardless of the deposition process. The deposit produced by CMT-P-Adv generally shows superior mechanical properties when compared to material deposited by CMT-P except for vertical orientation where in rolled and rolled & heat treated conditions CMT – P shows much better results as compared to CMT-P-Adv. The results in the horizontal section are used to investigate the impact of rolling on the material properties because this direction is considerably less impacted by defect alignment phenomenon than the vertical direction.

3.4.1. Horizontal direction

Fig. 9 provides plots of the horizontal tensile properties.

Rolling increases the 0.2% PS (+51%) and UTS (+22%) without affecting the elongation when applied to CMT-P-Adv material. Similarly, for the CMT-P material, rolling increases the UTS by 20% and the YS by 24%, but also significantly improves the elongation. This mechanical performance improvement is likely to be due to a combination of the reduction of the defect level and the improved response toward natural aging of the rolled material caused by the size reduction of second phases.

Heat treatment of the un-rolled material increases the 0.2% PS and UTS for both deposits but has little effect on the elongation. In this condition, the PS is similar for both deposits, but the maximum measured strength and elongation were considerably higher for the CMT-P-Adv deposit.

When applied to rolled material, heat treatment slightly reduces the 0.2% PS of the CMT-P-Adv material but raises the 0.2% PS of the CMT-P deposit. There is a large increase in elongation and UTS in both cases. The CMT-P-Adv deposit outperforms the material deposited by CMT-P by only 2% of elongation. For both processes, the properties achieved by rolled and heat treatment surpassed the un-rolled and un-rolled & heat-treated material.

The tensile properties in the vertical direction can be seen in Fig. 10. The trends observed in the horizontal direction were confirmed in this direction. For both processes, there was significant anisotropy, with both strength and elongation significantly lower in the vertical direction. This is due to the alignment of the pores along the layers previously reported by Qi et al. [13]. The significant difference between the horizontal and vertical direction is the elongation drop on the rolled CMT-P-Adv material, caused by the lack of bounding defects previously described and visible in Fig. 4.

Fig. 11 (a) shows a brittle rupture surface for the vertical rolled CMT-P-Adv specimen. After heat treatment, the rupture is much more ductile due to the dissolution of coarse Al_2Cu eutectic phases, as shown in Fig. 7. Numerous elliptic smooth areas are observed on the ruptured surface, as highlighted in green in Fig. 11 (b). The largest of these observed ellipses is 570 μm long and 220 μm wide. This defect shape and smooth surface suggests that these ellipses resulted from open pores partially closed during rolling, which offered no resistance toward crack propagation. These structures are not observed in the material tested in the horizontal direction. The fracture surfaces of all tested conditions were not included here for conciseness purpose, but these images are available in the supplementary data folder.

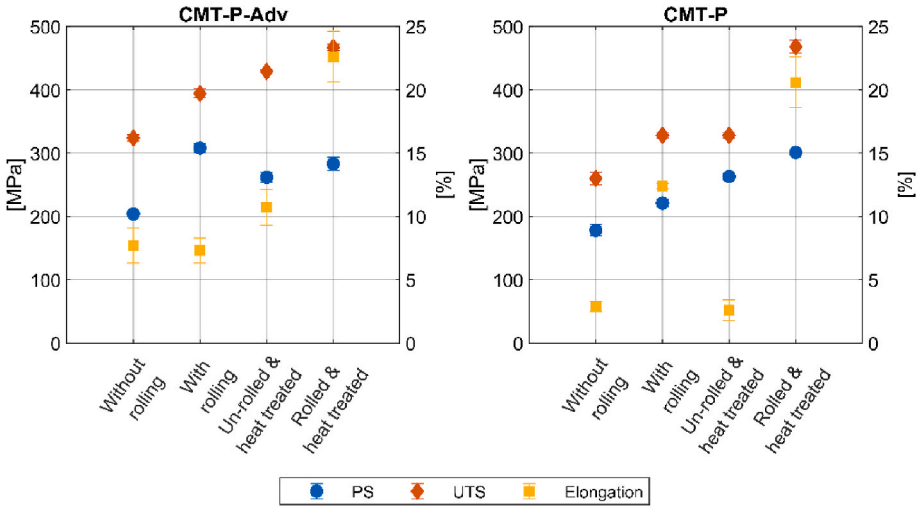

Fig. 9. Tensile properties measured in the horizontal direction for both processes in As-deposited (AD), As Rolled (AR), Heat Treated (HT) and Rolled then Heat treated (R & HT) conditions.

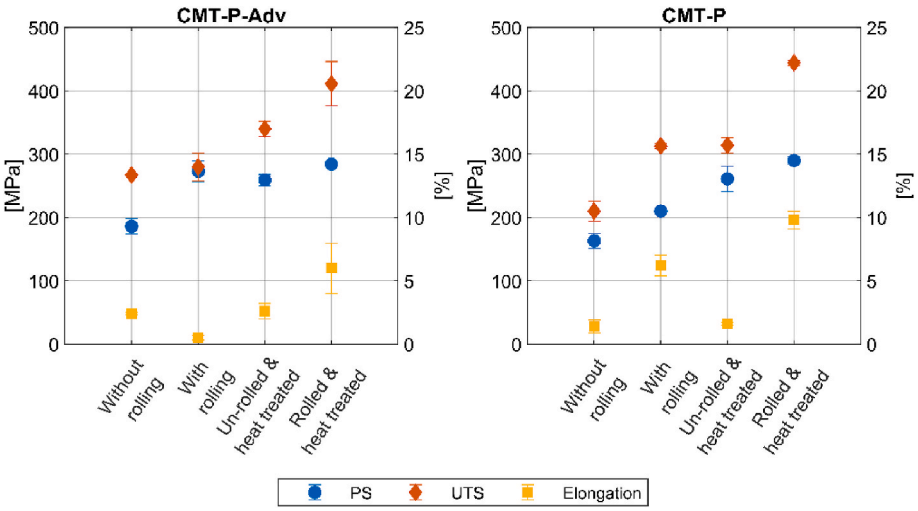

Fig. 10. Tensile properties measured in the vertical direction for both processes in As-deposited (AD), As Rolled (AR), Heat Treated (HT) and Rolled then Heat treated (R & HT) conditions.

Table 5
Tensile properties.

	As-deposited		As rolled		Heat treated		Rolled & heat treated	
	CMT-P-Adv	CMT-P	CMT-P-Adv	CMT-P	CMT-P-Adv	CMT-P	CMT-P-Adv	CMT-P
0.2% PS [MPa]								
Horizontal	204 ± 2	178 ± 9	308 ± 7	221 ± 6	262 ± 8	263 ± 5	283 ± 10	301 ± 1
Vertical	186 ± 12	163 ± 12	273 ± 16[b]	210 ± 5	259 ± 9	261 ± 20	284 ± 2	290 ± 6
UTS[a] [MPa]								
Horizontal	324 ± 5	260 ± 10	394 ± 7	328 ± 4	429 ± 2	328 ± 23	467 ± 5	468 ± 10
Vertical	267 ± 1	210 ± 16	280 ± 22	313 ± 4	340 ± 12	314 ± 12	411 ± 35	444 ± 4
Elongation [%]								
Horizontal	7.7 ± 1.4	2.9 ± 0.4	7.3 ± 1.0	12.4 ± 0.2	10.7 ± 1.4	2.6 ± 0.8	22.6 ± 2.0	20.6 ± 2.0
Vertical	2.4 ± 0.1	1.4 ± 0.5	0.5 ± 0.2	6.2 ± 0.8	2.6 ± 0.6	1.6 ± 0.1	6.0 ± 2.0	9.8 ± 0.7

[a] For the low ductility samples, the data provided as the UTS is the maximum strength measured during the test.
[b] The 0.2% PS measured for this sample is not representative of the material performances as the sample barely yield during the test, making it impossible to measure an accurate PS value.

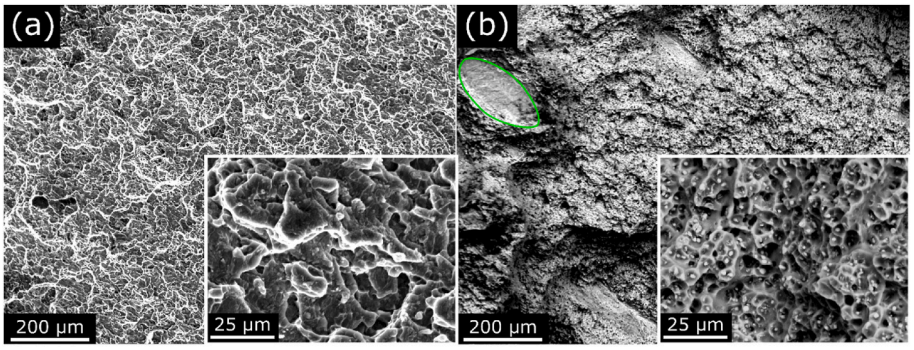

Fig. 11. SEM images of the fracture surface of vertical specimens deposited with the CMT-P-Adv process in the (a) as rolled and (b) rolled and heat treated conditions.

4. Discussion

4.1. Bead shape and microstructure

As reported in the literature, heat input drastically impacts the bead shape in WAAM deposition [26]. The higher bead aspect ratio and re-melted factor and the lower surface waviness of the wall deposited with CMT-P can be explained by the higher heat input of this process compared to CMT-P-Adv (234 J/mm against 120 J/mm; respectively). This difference in as-deposited geometry also explains why, despite using the same 45 kN rolling load, the percentage of deformation induced by rolling is so widely different (see Table 2).

The CMT-P-Adv process leads to a better deposition quality than the CMT-P process, with fewer dendritic shrinkage and gas pores. This lower porosity can be attributed to the alternating current and voltage profiles, typical of CMT advanced processes, which are well known for their wire cleaning role, leading to a lower porosity level in the deposited state. This is attributed to the wire oxide cleaning action of the arc when the wire is the cathode and the substrate the anode [26].

As illustrated by the re-melted coefficient in Table 2, the material

deposited with the CMT-P process endures numerous partial re-melting and reheating cycles because of the smaller LH to re-melted depth ratio than for the CMT-P-Adv process. In multi-pass welding, it has been shown that successive re-melting and low cooling rate can lead to the formation of dendritic shrinkage pores [34]. These cavities were described by Talbot as a consequence of the difference of hydrogen solubility in the liquid and solid [23]. During the solidification, the hydrogen is expelled from the growing solid crystal into the liquid. The hydrogen concentration in the liquid rises until it is high enough to nucleate as a gas bubble. This hypothesis is coherent with the numerous voids in between dendrites observed in CMT-P material, shown in Fig. 8. During fusion welding, a standard recommendation to reduce dendritic shrinkage cavities is to use a lower heat input. The higher heat input of the CMT-P process combined with the numerous re-melting phases is the reason why numerous interdendritic pores can be observed in the un-rolled CMT-P deposit. In contrast, none were observed in the as-deposited CMT-P-Adv material.

4.2. Mechanical properties

4.2.1. As-deposited condition

The as-deposited hardness average value, provided in Table 4, did not depend on the process. However, a higher variability of the measurement carried out on CMT-P material was observed. This variability can be explained by the higher level of defects in this material. Despite the differences between CMT-P and CMT-P-Adv mentioned above, the two processes generate a relatively low cooling rate compared to thermal cycle required to solutionise the alloying elements, generally generated by water quench. Therefore, both processes produce a similar microstructure in term of second phase size and distribution. This is why the average hardness value was not affected by the change of process in un-rolled and non heat treated condition. The tensile properties of the material deposited by CMT-P-Adv were significantly higher than those of CMT-P material, as detailed in Table 5. The elongation and maximum strength observed changes can be attributed to the higher level of defects in the CMT-P material as shown in Fig. 8 (b and c).

The tensile properties in the vertical direction were significantly lower than in the horizontal direction, regardless of the deposition process used. Ruptured surfaces of the vertical specimens observed by SEM show a lower resistance to crack propagation and more defects than in the horizontal direction. Therefore, the anisotropy of the mechanical properties in the as-deposited condition can be attributed to the defect distribution since the re-melted zones (that contains the defect) would now be oriented perpendicular to the application of the load. This is coherent with the observation reported by Qi et al. [13]. The horizontal properties of the material deposited with CMT-P are close to the properties of AA2024 deposited by a tandem GTA system [15].

4.2.2. Effect of inter-pass rolling

As shown by the hardness measurements reported in Table 4 and the tensile properties in Table 5, the inter-pass rolling effect depends on the deposition process used.

The hardness measurements provided in Table 4 clearly show that the effect of rolling depends on the deposition process. The un-changed hardness of the CMT-P material suggests that interlayer rolling did not strengthen the material through grain refinement, high density dislocations, fine sub-grains or precipitation hardening. However, the microstructure images, porosity data, and tensile properties show that inter-layer rolling impacted the material. The drastic reduction of defect level in the material can explain the increase in elongation, PS and UTS in both directions.

In the present study, the CMT-P rolled material is not strengthen by inter-pass rolling. Does not have a high dislocation density, as highlighted by the hardness value. This is likely to be due to the numerous reheating and re-melting cycles experienced by the material and a low deformation rate caused by the as-deposited geometry of the wall. However, the mechanical properties improvement suggests a higher response toward natural aging and the microstructure images show that the porosity and defect level is considerably reduced. It suggests that, in this case, the hydrogen is not stored in the dislocation but is released through dislocation pipes. It could also be trapped in grain boundaries. Indeed, most studies on the effect of deformation on the porosity of aluminium alloys were conducted on cast alloys, mainly composed of large grains. During these studies, grain boundaries were often considered a negligible trapping site, capable of storing 10 to 100 times less hydrogen than dislocation [35]. However, WAAM material is composed of much smaller grain, especially when inter-pas rolling is carried out. It means that there are many more grain boundaries in rolled WAAM material than in wrought alloys: grain boundary areas could also play a key role in hydrogen storing.

The rolled 2024 CMT-P-Adv material hardness increased considerably compared with the as-deposited material, as observed by Gu et al. for the 2319 alloys [16]. For 2319, the main rolling strengthening mechanisms identified were high-density dislocations and fine sub-grains with relatively low misorientations, as detailed in the first point of the introduction section focused on published finding on rolling of aluminium w-DED deposit. However, it has been shown that plastic deformations can have significant effect on the mechanical properties of the 2024 alloys by altering their precipitation behaviour after rolling. Zhao et al. showed the complicated relationship between the tensile properties of AA2024 and its thermochemical history [36]. Three types of precipitates play a crucial role in the strengthening of 2024 alloys: Al_2Cu, Al_2CuMg and Ω. The Ω phases are highly sensitive to strain and might form on specific crystallographic planes. The hardness after rolling the CMT-P-Adv material is close to the hardness obtained from heat treatment of the as-deposited structure. Such increment for a precipitation strengthening alloy cannot be solely attributed to microstructural features. Therefore, it is probable that, in addition to generating dislocations, inter-pass rolling also changes the precipitation behaviour of 2024 alloy, leading to improved mechanical properties when the CMT-P-Adv process is used. The absence of strengthening of the CMT-P material can be explained by a combination of two phenomena. The high heat input causes severe alloying element segregation, reducing the content of the alloying element in the matrix. This drastically reduce the natural aging response of the material. Also, the percentage of deformation generated by rolling for the CMT-P material was low because of the difference of as-deposited wall geometry.

The extremely low ductility in the vertical direction can be explained by apparently closed pores and the lack of bonding between layers, as suggested by the rupture surface and the literature [22]. The presence of unclosed pore, as observed in Fig. 11 (b) can be explained by a combination of the lower strain applied by rolling due to the bead geometry, and insufficient reheating. As demonstrated by Toda et al. [22] both high strain and post plastic deformation temperature are required to close pores. The lack of bonding between the folds of material on the side of the wall could behave as a stress concentration point and offer low resistance toward crack propagation, as suggested by the rupture surface shown in Fig. 11 (a). Unfortunately, these defects were not detected by μCT to confirm this hypothesis. The higher deformation rate of the CMT-P-Adv deposit, as detailed in Table 2, is also likely to contribute to lowering the UTS to 0.2% PS ratio.

4.2.3. Effect of heat treatment

Only one heat treatment was carried out in this study, and as mentioned before, it may not have been optimum. As shown by Qi et al. [15], the properties of 2024 manufactured by WAAM can be improved by heat treatment, and the temperature of the solution treatment is a key factor regarding the maximum properties achievable. Therefore, the work conducted here is not conclusive on the highest mechanical properties achievable with this alloy after heat treatment. However, heat treatment impact was investigated, and the effect of the deposition process and inter-pass rolling on the heat-treated mechanical properties

can be reported.

As for the effect of inter-pass rolling, the effect of heat treatment is different if it is carried out on CMT-P-Adv or CMT-P deposited material. The anisotropy, observed for both deposition processes, can be explained by the alignment of pores in the inter-layer boundary. These pores are more numerous after heat treatment than in the as-deposited condition, as observed by Qi et al. [13]. The effect of heat treatment is more mitigated when carried out on CMT-P material. This is due to the higher concentration of defect on the as-deposited material.

When heat treatment is carried out on the rolled CMT-P-Adv material, it does not affect the PS considerably, but the UTS and the elongation drastically increase. The material is still anisotropic despite a considerable increase in ductility in the vertical direction. However, the presence of un-closed, or re-opened, pores in the inter-layer boundary has a drastic effect on the rupture behaviour of the vertical specimens, as shown by the SEM image of the rupture surface in Fig. 11. It considerably affected the UTS and elongation measured in the vertical direction, generating a large measurement dispersion.

Inter-pass rolled & heat treated 2024 deposited with CMT-P process reaches the highest mechanical properties of all the conditions evaluated in this study, with a slightly higher PS than the material deposited with CMT-P-Adv. The anisotropy of this material is marginally lower than this of CMT-P-Adv material. That can be explained by the lower level of defect, and anisotropy of the material before heat treatment. However, the elongation in the vertical direction remains low, below 10%. The PS and hardness of the rolled and heat-treated material were considerably higher than these of the un-rolled and heat-treated material. This suggests that inter-pass rolling reduce the size of the Al_2Cu phases, making it easier to put them in solution and improving the material response to the solution treatment.

5. Conclusions

The present study demonstrated the deposition process's effect on the geometry, microstructure, and mechanical properties of 2024 WAAM inter-pass rolled material. The key findings that can be drawn from this study are the following:

1. The process input energy has a considerable effect on the geometry of the deposit and the re-melting depth which subsequently affects the efficacy of the rolling process. However, it has no significant impact on the strength of the as-deposited material.
2. The lower energy and alternating current process produces a deposit of higher strength and elongation than the higher energy process due to the formation of internal defects in the material deposited with the higher energy process.
3. The material response toward inter-pass rolling depends on the deposition process heat input. The low heat input process generated, after rolling, a strengthened matrix. However, the strength of the material deposited with the high heat input process increases only because of the drastic reduction of defect level. In both cases, the strength and elongation were improved, unless the bead geometry is such that lack of fusion defects are generated through the material folding over itself.
4. Heat treatment improves the microstructure and therefore strength of both the un-rolled and rolled material. It has little effect on porosity and therefore elongation.
5. The properties of WAAM 2024 can be significantly improved by combining cold work and post-deposition heat treatment. Application of these two processes enable drastic reduction of defects, resulting in a lower anisotropy and a higher ductility of the material than heat-treated material without inter-pass rolling.

For future studies on the combined effect of the deposition process and cold work on w-DED deposit, a process with flexible control of the deposition parameters would be required. The study could be repeated with a controlled layer height to re-melted depth or controllable heat input, independent from the deposition rate, using such deposition processes. Using innovative deposition processes, such as wire laser arc additive manufacture of alternating current plasma will enable a deeper understanding of the inter-dependant effect of the deposition process and cold work in aluminium WAAM.

Supplementary materials

The tensile test campaign results and the micro hardness measurement are available online at the DOI 10.17862/cranfield.rd.12143805.

Funding

This research work is supported by the Engineering and Physical Sciences Research Council (EPSRC) through the NEw Wire Additive Manufacturing (NEWAM) (grant number EP/R027218/1) research programme and by C-TEC, Constellium Technology Center.

CRediT authorship contribution statement

E. Eimer: Conceptualization, Methodology, Investigation, Writing – original draft, Writing – review & editing. **S. Ganguly:** Writing – review & editing. **S. Czink:** Methodology, Investigation, Writing – original draft, Writing – review & editing. **S. Dietrich:** Methodology, Resources, Writing – review & editing. **B. Chehab:** Resources, Writing – review & editing, Supervision, Funding acquisition. **J. Ding:** Conceptualization, Methodology, Resources, Writing – review & editing, Supervision, Funding acquisition. **S. Williams:** Conceptualization, Methodology, Resources, Writing – review & editing, Supervision, Funding acquisition.

Declaration of competing interest

The authors declare that they have no known competing financial interests or personal relationships that could have appeared to influence the work reported in this paper.

Data availability

The tensile test campaign results and the micro hardness measurement are available online at the DOI 10.17862/cranfield.rd.12143805

Acknowledgement

The authors would like to thank Nisar Shan, Flemming Nielsen, and John Thrower for their technical support during the manufacture of the samples; Steve Pope, Tracey Robert, and Christine Kimpton for their support during the metallography analysis phase of this work; and Ben Hopper and Andrea Giampiccolo for their support with the tensile testing campaign.

References

[1] S.W. Williams, F. Martina, A.C. Addison, J. Ding, G. Pardal, P. Colegrove, Wire+Arc Additive manufacturing, Mater. Sci. Technol. 32 (7) (2016) 641–647, https://doi.org/10.1179/1743284715Y.0000000073.

[2] A.S. Haselhuhn, M.W. Buhr, B. Wijnen, P.G. Sanders, J.M. Pearce, Structure-property relationships of common aluminum weld alloys utilized as feedstock for GMAW-based 3-D metal printing, Mater. Sci. Eng. 673 (2016) 511–523, https://doi.org/10.1016/j.msea.2016.07.099.

[3] Gu J., Wang X., Bai J., Ding J., Williams S., Zhai Y., et al. Deformation microstructures and strengthening mechanisms for the wire+arc additively manufactured Al-Mg4.5Mn alloy with inter-layer rolling. Mater. Sci. Eng.. Elsevier B.V.; 2018; 712(November 2017): 292–301. Available at: DOI:10.1016/j.msea.2017.11.113.

[4] K.F. Ayarkwa, S.W. Williams, J. Ding, Assessing the effect of TIG alternating current time cycle on aluminium wire + arc additive manufacture, Addit. Manuf. 18 (2017) 186–193, https://doi.org/10.1016/j.addma.2017.10.005. Elsevier B.V.

[5] E.A. Starke, J.T. Staleyt, Application of modern aluminum alloys to aircraft, Prog. Aero. Sci. 32 (95) (1996) 131–172, https://doi.org/10.1016/0376-0421(95)00004-6.
[6] B.N. Bhat, Aerospace Materials Characteristics. Aerospace Materials and Applications, American Institute of Aeronautics and Astronautics, 2018, pp. 11–207, https://doi.org/10.2514/5.9781624104893.0011.0208.
[7] S. Kou, A simple index for predicting the susceptibility to solidification cracking, Weld. J. 94 (2015) 374–388. December.
[8] C.G. Pickin, S.W. Williams, P.B. Prangnell, J. Robson, M. Lunt, Control of weld composition when welding high strength aluminium alloy using the tandem process, Sci. Technol. Weld. Join. 14 (8) (2009) 734–739, https://doi.org/10.1179/136217109X12505932584817.
[9] C.G. Pickin, S.W. Williams, P.B. Prangnell, J. Robson, M. Lunt, C. Derry, et al., Control of weld composition when arc welding high strength aluminium alloys using multiple filler wires, Sci. Technol. Weld. Join. 15 (6) (2010) 491–496, https://doi.org/10.1179/136217110X12785889549660.
[10] Qi Z., Cong B., Qi B., Sun H., Zhao G., Ding J. Microstructure and mechanical properties of double wire + arc additively manufactured Al Cu Mg alloys. J. Mater. Process. Technol.. Elsevier; 2018; 255(August 2017): 347–353. Available at: DOI: 10.1016/j.jmatprotec.2017.12.019.
[11] J. Gu, J. Bai, J. Ding, S. Williams, L. Wang, K. Liu, Design and cracking susceptibility of additively manufactured Al-Cu-Mg alloys with tandem wires and pulsed arc, J. Mater. Process. Technol. 262 (May) (2018) 210–220, https://doi.org/10.1016/j.jmatprotec.2018.06.030. Elsevier.
[12] J. Fixter, J. Gu, J. Ding, S.W. Williams, P.B. Prangnell, Preliminary investigation into the suitability of 2xxx alloys for wire-Arc Additive manufacturing, Mater. Sci. Forum. Scientifis.net (2017) 611–616, 10.4028, www.scientific.net/MSF.877.611.
[13] Z. Qi, B. Qi, B. Cong, H. Sun, G. Zhao, J. Ding, Microstructure and mechanical properties of wire + arc additively manufactured 2024 aluminum alloy components: as-deposited and post heat-treated, J. Manuf. Process. 40 (February) (2019) 27–36, https://doi.org/10.1016/j.jmapro.2019.03.003. Elsevier.
[14] J.R. Davis, Heat treating of aluminum alloys, in: A. International (Ed.), Metals Handbook, Desk Edition (second ed., ASM International, 1998, pp. 1032–1039.
[15] Z. Qi, B. Cong, B. Qi, J. Ding, Properties of wire + arc additively manufactured 2024 aluminum alloy with different solution treatment temperature, Mater. Lett. 230 (2018) 275–278, https://doi.org/10.1016/j.matlet.2018.07.144.
[16] J. Gu, J. Ding, S.W. Williams, H. Gu, J. Bai, Y. Zhai, et al., The strengthening effect of inter-layer cold working and post-deposition heat treatment on the additively manufactured Al– 6.3-Cu alloy, J. Mater. Process. Technol. 230 (2016) 26–34, https://doi.org/10.1016/j.jmatprotec.2015.11.006. Elsevier. (Accessed 14 April 2016).
[17] J. Gu, J. Ding, S.W. Williams, H. Gu, P. Ma, Y. Zhai, The effect of inter-layer cold working and post-deposition heat treatment on porosity in additively manufactured aluminum alloys, J. Mater. Process. Technol. 230 (2016) 26–34, https://doi.org/10.1016/j.jmatprotec.2015.11.006.
[18] J.R. Honnige, P.A. Colegrove, S. Ganguly, E. Eimer, S. Kabra, S. Williams, Control of residual stress and distortion in aluminium wire + arc additive manufactured with rolling, Addit. Manuf. 22 (2018) 775–783, https://doi.org/10.1016/j.addma.2018.06.015.
[19] P.a. Colegrove, H.E. Coules, J. Fairman, F. Martina, T. Kashoob, H. Mamash, et al., Microstructure and residual stress improvement in wire and arc additively manufactured parts through high-pressure rolling, J. Mater. Process. Technol. 213 (10) (2013) 1782–1791, https://doi.org/10.1016/j.jmatprotec.2013.04.012. Elsevier B.V.
[20] F. Martina, S.W. Williams, P. Colegrove, Improved microstructure and increased mechanical properties of additive manufacture produced Ti-6Al-4V by interpass cold rolling, SFF Symp. (2013) 490–496, https://doi.org/10.1007/s13398-014-0173-7.2.
[21] J.R. Honnige, P.A. Colegrove, B. Ahmad, M.E. Fitzpatrick, S. Ganguly, T.L. Lee, et al., Residual Stress and Texture Control in Ti6Al4V Wire + Arc Additively Manufactured Intersections by Stress Relief and Rolling. Materials and Design, vol. 150, Elsevier Ltd, 2018, pp. 193–205, https://doi.org/10.1016/j.matdes.2018.03.065.
[22] H. Toda, K. Minami, K. Koyama, K. Ichitani, M. Kobayashi, K. Uesugi, et al., Healing behavior of preexisting hydrogen micropores in aluminum alloys during plastic deformation, Acta Materialia. Acta Materialia Inc. 57 (15) (2009) 4391–4403, https://doi.org/10.1016/j.actamat.2009.06.012.
[23] D.E.J. Talbot, Effects of hydrogen in aluminium, magnesium, copper, and their alloys, Int. Metall. Rev. 20 (1) (1975) 166–184, https://doi.org/10.1179/imtlr.1975.20.1.166.
[24] O. Kubaschewski, Gases and Metals, 1970.
[25] K.F. Ayarkwa, S. Williams, J. Ding, Investigation of pulse advance cold metal transfer on aluminium wire arc additive manufacturing, Int. J. Rapid Manuf. 5 (1) (2015) 44–57.
[26] B. Cong, J. Ding, S.W. Williams, Effect of arc mode in cold metal transfer process on porosity of additively manufactured Al-6.3%Cu alloy, Int. J. Adv. Des. Manuf. Technol. 76 (9–12) (2014) 1593–1606, https://doi.org/10.1007/s00170-014-6346-x.
[27] E.M. Ryan, T.J. Sabin, J.F. Watts, M.J. Whiting, The influence of build parameters and wire batch on porosity of wire and arc additive manufactured aluminium alloy 2319, J. Mater. Process. Technol. 262 (July) (2018) 577–584, https://doi.org/10.1016/j.jmatprotec.2018.07.030. Elsevier.
[28] B. Cong, J. Ding, S. Williams, Effect of arc mode in cold metal transfer process on porosity of additively manufactured Al-6.3%Cu alloy, Int. J. Adv. Manuf. Technol. 76 (9–12) (2015) 1593–1606, https://doi.org/10.1007/s00170-014-6346-x.
[29] The Aluminium Association, International Alloy Designations and Chemical Composition Limits for Wrought Aluminum and Wrought Aluminum Alloys with Support for On-Line Access from: Aluminum Extruders Council Use of the Information, The Aluminum Association, Arlington, Virginia, 2015, p. 31. Enero 2015.
[30] J.N. Dupont, A.R. Marder, Thermal efficiency of arc welding processes, Weld. Res. Suppl. 74 (December) (1995) 406–416, https://doi.org/10.1016/j.jmatprotec.2014.12.002. Available at:.
[31] J.G. Kaufman, Aluminum alloy database: table 4b. Typical physical properties of wrought aluminum alloys (metric units), Knovel (2015) 4–5. https://app.knovel.com/hotlink/itble/rcid:kpAAD00001/id:kt00UBBRY2/aluminum-alloy-database/table-4b-typical-physical. (Accessed 12 January 2023).
[32] X. Xu, J. Ding, S. Ganguly, S. Williams, Investigation of process factors affecting mechanical properties of INCONEL 718 superalloy in wire + arc additive manufacture process, J. Mater. Process. Technol. 265 (2019) 201–209, https://doi.org/10.1016/j.jmatprotec.2018.10.023. Elsevier.
[33] J. Gu, M. Gao, S. Yang, J. Bai, J. Ding, X. Fang, Pore formation and evolution in wire + arc additively manufactured 2319 Al alloy, Addit. Manuf. 30 (October) (2019), 100900, https://doi.org/10.1016/j.addma.2019.100900. Elsevier.
[34] S. Kou, Difficulties Associated with the Partially Melted Zone. Weld. Metall, second ed. second ed., John Wiley & Sons, Inc, 2003, pp. 321–340.
[35] H. Toda, H. Oogo, K. Uesugi, M. Kobayashi, Roles of pre-existing hydrogen micropores on ductile fracture, Mater. Trans. 50 (9) (2009) 2285–2290, https://doi.org/10.2320/matertrans.M2009123.
[36] Y.L. Zhao, Z.Q. Yang, Z. Zhang, G.Y. Su, X.L. Ma, Double-peak age strengthening of cold-worked 2024 aluminum alloy, Acta Mater. 61 (5) (2013) 1624–1638, https://doi.org/10.1016/j.actamat.2012.11.039.